Current Research in Food Science 8 (2024) 100668

Contents lists available at ScienceDirect

Current Research in Food Science

journal homepage: www.sciencedirect.com/journal/current-research-in-food-science

Inclusion complex of turmeric essential oil with hydroxypropyl-β-cyclodextrin: Preparation, characterization and release kinetics

Yueyue Qiang [a,b], Hang Wei [a], Biao Huang [a], Hongfei Chi [a,b], Jianwei Fu [a,b,*]

[a] Institute of Quality Standards & Testing Technology for Agro-products, Fujian Academy of Agricultural Sciences/ Fujian Key Laboratory of Agro-products Quality and Safety, Fuzhou, 350003, China
[b] College of Food Science, Fujian Agriculture and Forestry University, Fuzhou, 350002, China

ARTICLE INFO

Handling Editor: Dr. Xing Chen

Keywords:
Turmeric essential oil
Inclusion complex
Characterization
Release kinetics

ABSTRACT

The application of turmeric essential oil (TEO), a natural effective antibacterial agent, in food preservation is limited due to high volatility and low stability. This study aimed to improve its stability and release behavior by synthesizing TEO/hydroxypropyl-β-cyclodextrin (HP-β-CD) inclusion complex (IC) in a saturated aqueous solution. An orthogonal experimental design was used to determine the optimal process conditions (HP-β-CD to TEO, g/mL), 16:1; stirring speed, 850 r/min; encapsulation time, 2 h), achieving a comprehensive score value of 85.62% for TEO/HP-β-CD-IC. Through comprehensive characterization, the results showed that TEO was completely embedded in HP-β-CD with increased stability. Free TEO exhibited a weight loss of 67.64% between 30 and 300 °C, while TEO/HP-β-CD-IC had a mass loss of only 9.33%. HP-β-CD and TEO/HP-β-CD-IC showed positive ZP values that were 124.76 mV and 132.16 mV, respectively. The release behavior and release kinetics of TEO/HP-β-CD-ICs were also studied, and the results showed that TEO/HP-β-CD-IC release rate increased under higher temperature and relative humidity—consistent with Fick's diffusion.

1. Introduction

Turmeric (*Curcuma longa* L.), a perennial herb, has been widely used in Asia as a safe and edible medicine, spice, and food additive (Chumroenphat et al., 2021). Turmeric essential oil (TEO), the main turmeric metabolite, is the key contributor to its pharmacological effects (Ferreira et al., 2013). Generally, essential oils (EOs) have great application potential in different fields, but their high volatility, poor water solubility, and sensitivity to the environmental components (e.g., light, oxygen, heat, pressure, and chemicals) limit their applications in different fields (De Santana et al., 2020; Shetta et al., 2019). A suitable method to protect TEO from evaporation and degradation and improve their stability is therefore needed urgently. Encapsulation is one of the most effective technologies for improving the stability, masking the taste or odor, and extending the shelf life of a food product. Microencapsulation of TEO in capsules using an appropriate wall material can help prevent adverse reactions and effects of environmental conditions during storage (Mehran et al., 2020). Several researchers have reported that alginate, chitosan, or cassava starch can be used for turmeric EO (TEO) encapsulation and controlled release (Lertsutthiwong et al., 2008, 2009; Li et al., 2019; Mustapha et al., 2019). However, these methods have the limitations of low loading capacity and poor release. To address this issues, we fabricated a TEO/hydroxypropyl-β-cyclodextrin (HP-β-CD) inclusion complex (IC) to enable TEO encapsulation and controllable delivery. To our knowledge, there are few reports on embedding TEO with HP-β-CD. HP-β-CD is a cyclic oligosaccharide containing seven D-(+) -glucopyranose units with a circular structure of hydrophobic cavity and a hydrophilic external structure. Compared with natural cyclodextrins (CDs), HP-β-CD can provide a more convenient complexation process due to its structure and amorphous nature (Adhikari et al., 2018). Furthermore, HP-β-CD is a hydroxyalkyl derivative, which can also be used as a substitute for α-CD, β-CD, or γ-CD to increase water solubility, complexation ability, and toxicological property (Gould and Scott, 2005).

EOs are commonly used for food preservation due to their antibacterial and antioxidant properties. Several studies have shown that EOs

* Corresponding author. Institute of Quality Standards & Testing Technology for Agro-products, Fujian Academy of Agricultural Sciences/ Fujian Key Laboratory of Agro-products Quality and Safety, No. 247, Wusi Road, Gulou District, Fuzhou, Fujian, 350003, China.
E-mail address: fjw9238@163.com (J. Fu).

https://doi.org/10.1016/j.crfs.2023.100668
Received 16 September 2023; Received in revised form 16 December 2023; Accepted 18 December 2023
Available online 30 December 2023

can prolong the shelf life of food and maintain food quality, which were affected by the release characteristics of EOs from the IC (Li et al., 2020; Zhou et al., 2021). However, the release behavior and release kinetics of TEO embedded in HP-β-CD during long-term storage under different relative humidity (RH) and temperature conditions remain unknown.

The current study aimed to encapsulate TEO in HP-β-CD to enhance its stability, thus increasing its applicability in various industries, especially the food industry. TEO was encapsulated in HP-β-CD using a saturated aqueous solution method and the prepared TEO/HP-β-CD-IC were optimized using an orthogonal design and then characterized. Finally, several release kinetic models were used to study the release behavior of TEO/HP-β-CD-IC at different temperatures and RH. This study has laid a theoretical and experimental basis for applying TEO/HP-β-CD-IC in food preservation.

2. Materials and methods

2.1. Materials

Turmeric was procured from Jiangxi Zhangshu Tianqitang Traditional Chinese Medicine Pieces (Zhangshu, China), HP-β-CD from Shandong Binzhou Huike Cyclodextrin Technology (Binzhou, China), petroleum ether from Xilong Science (Shantou, China), and anhydrous sodium sulfate and methanol from Sinopharm Chemical Reagent (Shanghai, China). Moreover, sodium chloride, anhydrous calcium chloride, and anhydrous potassium carbonate were all purchased from Shanghai Macleans Biochemical Technology (Shanghai, China).

2.2. TEO/HP-β-CD-IC preparation

Briefly, turmeric was pulverized into a fine powder, followed by passing through an 80-mesh sieve and extracting TEO by hydrodistillation of 500 g of the sieved powder for 5 h using a double-layer glass reactor (S212-30L; Shanghai Yujie Instrument) (Commission, 2015). Next, the extracted TEO was collected and then mixed with anhydrous sodium sulfate (Na_2SO_4), followed by filtration, to remove any water remaining after extraction. This TEO was stored in sealed glass vials at 4 °C in dark before further use.

TEO/HP-β-CD-IC was prepared by dissolving a given mass of HP-β-CD in deionized water until saturation. Next, based on the different ratios of HP-β-CD and TEO in the orthogonal analysis table, the corresponding volume of TEO was dispersed in absolute ethyl alcohol, followed by adding it to the aqueous HP-β-CD solution and agitating the mixture at 40 °C with a magnetic stirrer at the indicated time period and speed for the experiments. After cooling the mixture at 4 °C in a refrigerator for 24 h, TEO/HP-β-CD-IC was obtained by centrifugal separation, and the precipitate was washed with petroleum ether, followed by filtration and freeze-drying until a constant weight.

2.2.1. Optimization of TEO/HP-β-CD-IC formulation

Orthogonal design can be used for rapid and economical selection of some representative points as test points (Yang et al., 2015). In this experiment, TEO/HP-β-CD-IC was prepared by the saturated aqueous solution method, and an L_9 (3^4) orthogonal analysis was used to determine the optimal conditions for preparing TEO/HP-β-CD-IC, including the ratio of HP-β-CD to TEO (g/mL), stirring speed (r/min), and encapsulation time (h), which were selected as three influencing factors (marked as A, B, and C in Table S1, respectively).

2.2.2. Comprehensive score value (CSV)

Briefly, TEO (2 mL) was put into a 500-mL round bottom flask, followed by adding 300 mL of distilled water for TEO extraction. Blank recovery (BR) was calculated to be 78.0% by equation (1) (Wang et al., 2015).

$$\mathrm{BR}\ (\%) = \frac{V_C}{V_A} \times 100 \tag{1}$$

where *Vc* indicates the amount (mL) of TEO extracted; and V_A, amount (mL) of initially added TEO.

In order to determine IC rate, TEO/HP-β-CD-IC was placed in a round-bottomed flask, followed by adding 300 mL of purified water to extract TEO while accurately measuring the TEO content (mL) of TEO/HP-β-CD-IC. The IC rate of EO was determined by equation (2) (Wang et al., 2015).

$$\text{IC rate of TEO}\ (\%) = \frac{V_{IC}}{V_A \times \mathrm{BR}} \times 100 \tag{2}$$

where V_{IC} is the amount (mL) of measured TEO in TEO/HP-β-CD-IC; V_A, the amount (mL) of initially added TEO.

The yield of IC was defined as the ratio of TEO/HP-β-CD-IC to HP-β-CD and TEO. The yield of IC was determined by equation (3) (Wang et al., 2015).

$$\text{IC yield}\ (\%) = \frac{M_{IC}}{M_{CD} + M_{EO}} \times 100 \tag{3}$$

where M_{IC} is the amount (g) of the TEO/HP-β-CD-IC; M_{CD}, HP-β-CD amount (g) of initially added to the TEO/HP-β-CD-IC, and M_{EO}, TEO amount (g) initially added to the TEO/HP-β-CD-IC.

The experiment was conducted using the IC rate of TEO, with the yield of IC as an index. These indexes were given appropriate weight coefficients, resulting in a CSV for the optimal IC process. The IC rate of EO is an important index to measure the IC effect: The higher the IC rate, the better the IC effect of EO. Therefore, a weight coefficient of 0.5 was assigned to the IC rate of TEO. The IC yield also occupied an important position in the industry's actual production application, i.e., in the same amount of HP-β-CD, the greater the IC yield, the better the IC effect of TEO. Therefore, a weight coefficient of 0.5 was assigned to TEO here, and the CSV was determined by equation (4) (Liu et al., 2018; Wang et al., 2015).

$$\mathrm{CSV}\ (\%) = \text{IC rate of TEO} \times 0.5 + \text{IC yield} \times 0.5 \tag{4}$$

2.3. Physical and chemical characterization of TEO/HP-β-CD-IC

2.3.1. Preparation of a physical mixture of TEO and HP-β-CD

A TEO/HP-β-CD physical mixture (PM) was prepared as the control. We used a mortar and pestle to manually grind TEO and HP-β-CD for 15 min to make them uniform.

2.3.2. Scanning electron microscopy (SEM)

HP-β-CD and TEO/HP-β-CD-IC were examined through SEM at an accelerating voltage of 15 kV. Briefly, the prepared powders were first fixed to the aluminum post with a double-sided tape, followed by gold-plating with a sprayer (EIKO IB-5, Shanghai Platinum Scale Trading Co., Ltd, Shanghai, China) and observing the powders under a scanning electron microscope (JSM-6380LV, JEOL, Japan) at 300 × magnification.

2.3.3. ^1H nuclear magnetic resonance (NMR)

^1H NMR spectra of HP-β-CD and TEO/HP-β-CD-IC were obtained on an NMR spectrometer (AVANCE NEO 600, Bruker, Germany) at 600 MHz and 298 K. Before analysis, HP-β-CD and TEO/HP-β-CD-IC samples were dissolved in D_2O (Lima et al., 2019).

2.3.4. Particle size and Zeta potential (ZP)

Particle size and ZP were analyzed on a ZP and nanoparticle size analyzer (NanoPlus3, Micromeritics Instrument, USA). The dynamic light scattering method was used to measure the particle size under a backscattering detector at 633 nm, 25 °C, and 173°. The surface charge

at the interface of TEO/HP-β-CD-IC oil droplets was measured using the phase analysis light scattering method (Acevedo-Fani et al., 2015).

2.3.5. Fourier-transform infrared (FT-IR) spectroscopy

The FT-IR spectra of TEO, HP-β-CD, PM, and TEO/HP-β-CD-IC were collected from 400 to 4000 cm^{-1} on an FT-IR Spectrometer (AVATAR360, Thermo Nicolet Corporation, USA) with 32 scans at a 4 cm^{-1} resolution. Briefly, each sample was then diluted with potassium bromide (KBr) powder at a mass ratio of 1:100, followed by pressing the sample into the disc with a diameter of 8 mm, distributing the sample evenly on a piece of KBr window and clamping the sample with another piece of KBr window (Rakmai et al., 2017).

2.3.6. X-ray diffractometry (XRD)

X-ray diffraction patterns of TEO, HP-β-CD, PM, and TEO/HP-β-CD-IC were obtained on an X-ray diffractometer (DY1602, Malvern analytical, Netherlands) with a 40-kV, 40-mA copper target X-ray tube under Cu Kα radiation. All samples were measured at a 2θ angle of 5°–40°, a 0.02 step width and a 0.5 s/step counting time (Wei et al., 2017).

2.3.7. Differential scanning calorimetry (DSC)

DSC analysis of TEO, HP-β-CD, PM, and TEO/HP-β-CD-IC was performed using a simultaneous thermal analyzer under a dynamic nitrogen atmosphere (100 mL/min) in an aluminum crucible at a heating rate of 10 °C/min and a temperature range of 30–500 °C (~2 mg of each sample) (Lima, et al., 2019). Each set of the test was done in triplet.

2.3.8. Thermogravimetric analysis (TGA)

Thermal properties of TEO, HP-β-CD, PM, and TEO/HP-β-CD-IC were investigated on a simultaneous thermal analyzer (STA449F5, Germany Naichi Instrument Manufacturing, Germany). In a nitrogen atmosphere, a 10 mg sample was heated from room temperature to 500 °C at a heating rate of 10 °C/min (Yin et al., 2021). All samples were done in triplet.

2.4. Release kinetics of the TEO from TEO/HP-β-CD-IC

The influence of RH and temperature on the amount of TEO released by TEO/HP-β-CD-IC was evaluated using the method reported by Yin et al. (2021) with some modifications. Briefly, 3 g of calcium chloride (4, 27, and 40 °C), 3 mL of saturated potassium carbonate (4 and 27 °C), and saturated sodium chloride solution (4, 27, and 40 °C) were filled in a 70-mL glass vial with RH at 0%, 45%, and 75%, respectively. TEO/HP-β-CD-IC were stored under 75% RH at 40 °C in a constant climate chamber (PRX-250B, Ningbo Haishu Saifu Experimental Instrument Factory, Ningbo, China). Then, a 2-mL glass vial containing 0.1 g of TEO/HP-β-CD-IC was placed in a 70-mL glass vial, sealed, and stored at 4, 27, and 40 °C for 27, 20, and 9 days, respectively. Next, TEO/HP-β-CD-IC in the 2-mL glass vial was dissolved in 50% (v/v) methanol solution, and the amount of TEO released from the headspace was measured by spectrophotometry at 230 nm. The amount of TEO released was determined as the total amount of TEO in the TEO/HP-β-CD-IC at the beginning of storage minus that at the end of storage.

2.5. Statistical analysis

Statistical analyses were performed using SPSS 16.0 software (SPSS, Inc., Chicago, IL, USA). The figures were constructed using Origin 8.5 (Origin Lab, Northampton, MA, USA) and GraphPad Prism 8 (GraphPad Software, Boston, USA).

3. Results and discussion

3.1. Orthogonal design for optimal formulation selection

Table 1 shows experiment results of the L_9 (3^4) orthogonal design corresponding to four columns and nine rows. The IC yield and IC rate of TEO were calculated as CSVs for selecting the best process parameters.

As shown in Table 1, $R_C > R_A > R_B$, and the CSVs values were affected by the various factors in the following order of stirring time > ratio of HP-β-CD and TEO > encapsulation speed. The inclusion process was gradual, with guest molecules entering the molecular cavity of the inclusion material, followed by intermolecular interaction, indicating that time was an important factor affecting the inclusion effect. Generally, the molecular cavity provided by HP-β-CD cannot be completely occupied by the guest molecules and the ratio of the host and guest molecules in the IC has a greater influence on IC formation, i.e., the number of molecular cavities provided by the inclusion material increases in a host-guest molecular ratio-dependent manner, thereby increasing the probability of guest molecules being included or the inclusion rate. In this process, appropriate agitation favors the molecular movement of the inclusion material to suppress its intermolecular interaction and promote the full contact of the inclusion material with the guest molecules to facilitate their entry into the molecular cavity of the inclusion material.

The optimal level of the aforementioned three factors was determined by *K* values. Comparison of different *k* values revealed $A_3B_2C_3$ as the optimal prescription with a CSV of 85.62% under ratio of HP-β-CD and TEO (g/mL), 16:1; stirring speed, 850 r/min; encapsulation time, 2 h. The validation experiment was performed to determine if the TEO/HP-β-CD-IC prepared by the optimal process had the highest combined score. The combined score of TEO/HP-β-CD-IC prepared by the $A_3B_2C_3$ process conditions was 86.12%, which was higher than the optimal value in the results of the orthogonal test protocol.

3.2. Characterization of TEO/HP-β-CD-IC

3.2.1. SEM analysis

Morphological examination is a qualitative technique for observing the surface structure of raw materials or prepared formulation. The SEM images of HP-β-CD and TEO/HP-β-CD-IC are shown in Fig. 1A-B, respectively. The inclusion process may change HP-β-CD morphology, so the morphological differences before and after HP-β-CD inclusion indicate IC formation (Rakmai et al., 2017). Here, the typical morphology of

Table 1
Orthogonal experiment design and results.

No.	Factors			IC rate of TEO (%)	IC yield (%)	CSV (%)
	A* (g/mL)	B* (r/min)	C* (h)			
1	3	3	1	94.58	52.60	73.59
2	1	2	3	95.74	73.91	84.83
3	3	1	3	95.27	67.95	81.61
4	1	3	2	95.50	72.27	67.97
5	2	3	3	95.22	69.00	82.11
6	3	2	2	95.48	68.68	82.08
7	2	2	1	97.20	67.45	82.32
8	2	1	2	97.79	61.24	79.52
9	1	1	1	97.55	73.09	85.32
K_1	238.12	246.45	241.23	–	–	–
K_2	243.95	249.22	229.57	–	–	–
K_3	246.92	243.45	248.54	–	–	–
k_1	79.37	82.15	80.41	–	–	–
k_2	81.32	83.07	76.52	–	–	–
k_3	82.31	81.15	82.85	–	–	–
R	2.93	1.93	6.32	–	–	–

Note: A denotes the ratio of HP-β-CD to TEO (g/mL); B, stirring speed (r/min); C, encapsulation time (h).

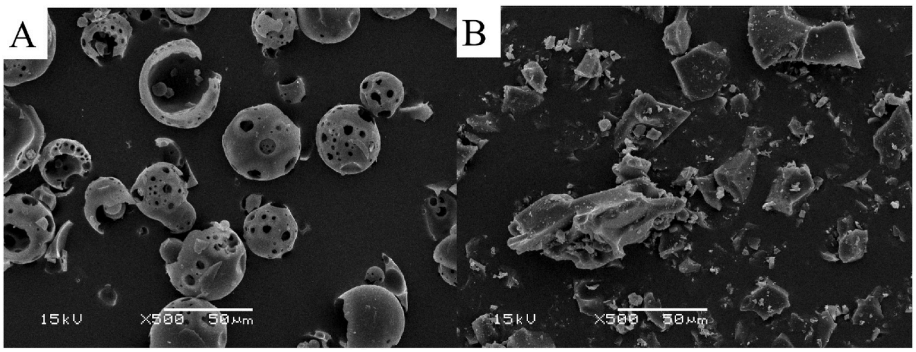

Fig. 1. SEM images of HP-β-CD (A) and TEO/HP-β-CD-IC (B; magnification, 500 ×).

HP-β-CD was reported as amorphous spherical particles with cavity structures (Lima, et al., 2019; Wei et al., 2017). However, the original form of HP-β-CD disappeared in TEO/HP-β-CD-IC, showing an irregular block structure. This significant change in particle morphology can be attributed not only to TEO–HP-β-CD interaction, but also to water loss during TEO/HP-β-CD-IC, leading to agglomeration (Lima, et al., 2019). Compared with HP-β-CD, TEO/HP-β-CD-IC presented a larger particle size, which is consistent with particle size analysis in the latter.

3.2.2. ^1H NMR analysis

NMR can be used to confirmed that guest and CD molecules have formed ICs because when guest molecules penetrate the cavity of CD, the chemical shift of CD changes. In addition, NMR can provide information about the molecular conformation of supramolecular structure and the direction of penetration of the guest molecules in the CD cavity (Yao et al., 2014). When the environment surrounding the H atoms in the CD cavity changes due to complexation with the guest molecules, the chemical shift of the CD changes. When the formation of ICs, H−5, and H−3 toward the inner cavity of CD chemically shifts, H−1, H−2, and H−4 atoms demonstrate chemical shifts toward the external cavity (Adhikari, et al., 2018).

Table 2 presents the values of the chemical shift difference between HP-β-CD protons in the presence and absence of TEO and the chemical shifts (δ) of free HP-β-CD and TEO/HP-β-CD-IC. In the free HP-β-CD spectrum, the shifts were shown to be 5.167, 3.506, 3.942, 3.412, and 3.789 ppm for H−1, H−2, H−3, H−4, and H−5, respectively, consistent with those reported in previous studies on flavonoids and HP-β-CD (Qiu, et al., 2014). However, in TEO/HP-β-CD-IC spectrum, the chemical shift of HP-β-CD changed somewhat relative to free HP-β-CD. In Tables 2 and it was shown that the chemical shift difference of H−2, H−3, and H−4 was small (−0.004, −0.003 and −0.001 ppm), in contrast to a relatively large chemical shift difference for H−1(−0.019 ppm) and H−5 (−0.012 ppm). H−1, H−2 and H−4 were located on the outer surface of HP-β-CD, whereas H−3 and H−5 were located in the cavity of HP-β-CD; H−3 was located at the large mouth end, and H−5 was located at the small mouth end (Wei, et al., 2017). The chemical shift value of the H−5 was larger than that of H−3. The results indicated that TEO entered the cavity of HP-β-CD molecule from the small mouth end, causing a large change in the external H−1 of HP-β-CD, which confirmed the formation of the TEO/HP-β-CD-IC.

Table 2
Main chemical shift values (δ) of HP-β-CD and TEO/HP-β-CD-IC.

Proton	HP-β-CD δ (ppm)	TEO/HP-β-CD-IC δ (ppm)	Δδ(ppm)
H−1	5.167	5.148	-0.019
H−2	3.506	3.502	-0.004
H−3	3.942	3.939	-0.003
H−4	3.412	3.411	-0.001
H−5	3.789	3.777	-0.012

Note: Δδ denotes chemical shift difference (i.e., changes).

3.2.3. Particle size and ZP analysis

The particle size distributions of HP-β-CD and TEO/HP-β-CD-IC are shown in Fig. 2A and Table S2. And the median diameters D_{50} were 204.3 nm and 644.6 nm for HP-β-CD and TEO/HP-β-CD-IC, respectively.

The surface charge of nanoparticles (NPs) is important for their targeted adsorption, bioavailability, and particle stability (Matshetshe et al., 2018). Table S2 presents the surface charge of HP-β-CD and TEO/HP-β-CD-IC. HP-β-CD and TEO/HP-β-CD-IC showed positive ZP values that were 124.76 mV and 132.16 mV, respectively. As reported by Wissing et al. (2004), an absolute ZP > 30 mV could provide good stability, whereas an absolute ZP of ~20 mM would provide short-term stability, with a fast aggregation observed at a ZP of 5 mV. It is worth mentioning that TEO/HP-β-CD-IC ZP values were significantly higher than HP-β-CD values indicating a superior stability.

3.2.4. FT-IR analysis

FT-IR is an important tool to confirm the complexation of TEO with HP-β-CD. Fig. 2B shows the FT-IR spectra of TEO, HP-β-CD, PM, and TEO/HP-β-CD-IC. HP-β-CD showed characteristic peaks at 3405 cm^{-1} (O–H stretching vibration), 2929 cm^{-1} (C–H stretching vibration), 1647 cm^{-1} (H–O–H bending vibration), 1157 cm^{-1} (C–O–C asymmetric stretching vibration), 1082 cm^{-1}(C–C stretching vibration), and 1031 cm^{-1} (C–O stretching vibration) (Yao et al., 2014). TEO demonstrated some characteristic peaks at 2873–3021 cm^{-1} (C–H stretching vibrations) (Ban et al., 2020). Moreover, the bands at 2963, 1686, 1448, and 1377 cm^{-1} represented C–H stretching vibration, C═C stretching, C–OH absorption bending vibration, and the CH_3 bend, respectively (Noghabi and Molaveisi, 2020), and the band at 878 cm^{-1} indicated = CH_2 bending vibration (out of plane). For the PM sample, more typical characteristic eigen peaks (1750–1000 cm^{-1}) belonging to TEO can still be observed, indicating that TEO and HP-β-CD are relatively dispersed in the PM sample. The spectra of TEO/HP-β-CD-IC and HP-β-CD were highly similar, with almost complete disappearance of characteristic absorption peaks of TEO, indicating that TEO molecules were embedded in the HP-β-CD cavity. Unlike the PM sample, since the TEO was embedded inside, the FT-IR test could only detect the functional groups on the surface of the HP-β-CD and might not detect the corresponding vibrational peaks of the TEO inside the HP-β-CD, and thus the characteristic peaks of the corresponding TEOs in the TEO/HP-β-CD-IC almost disappeared.

3.2.5. XRD analysis

The formation of TEO/HP-β-CD-IC was further investigated by its XRD patterns (Wei, et al., 2017). Specifically, the physical state of TEO after complexation with HP-β-CD was analyzed by XRD method, and Fig. 2C shows the XRD patterns of TEO, HP-β-CD, PM, and TEO/HP-β-CD-IC. TEO exhibited one characteristic peak at 2θ of 17.72°, while both HP-β-CD and TEO/HP-β-CD-IC had a different characteristic peak at 18.65°. Meanwhile, the amorphous HP-β-CD had no crystalline peak, and TEO/HP-β-CD-IC had no characteristic peak corresponding to

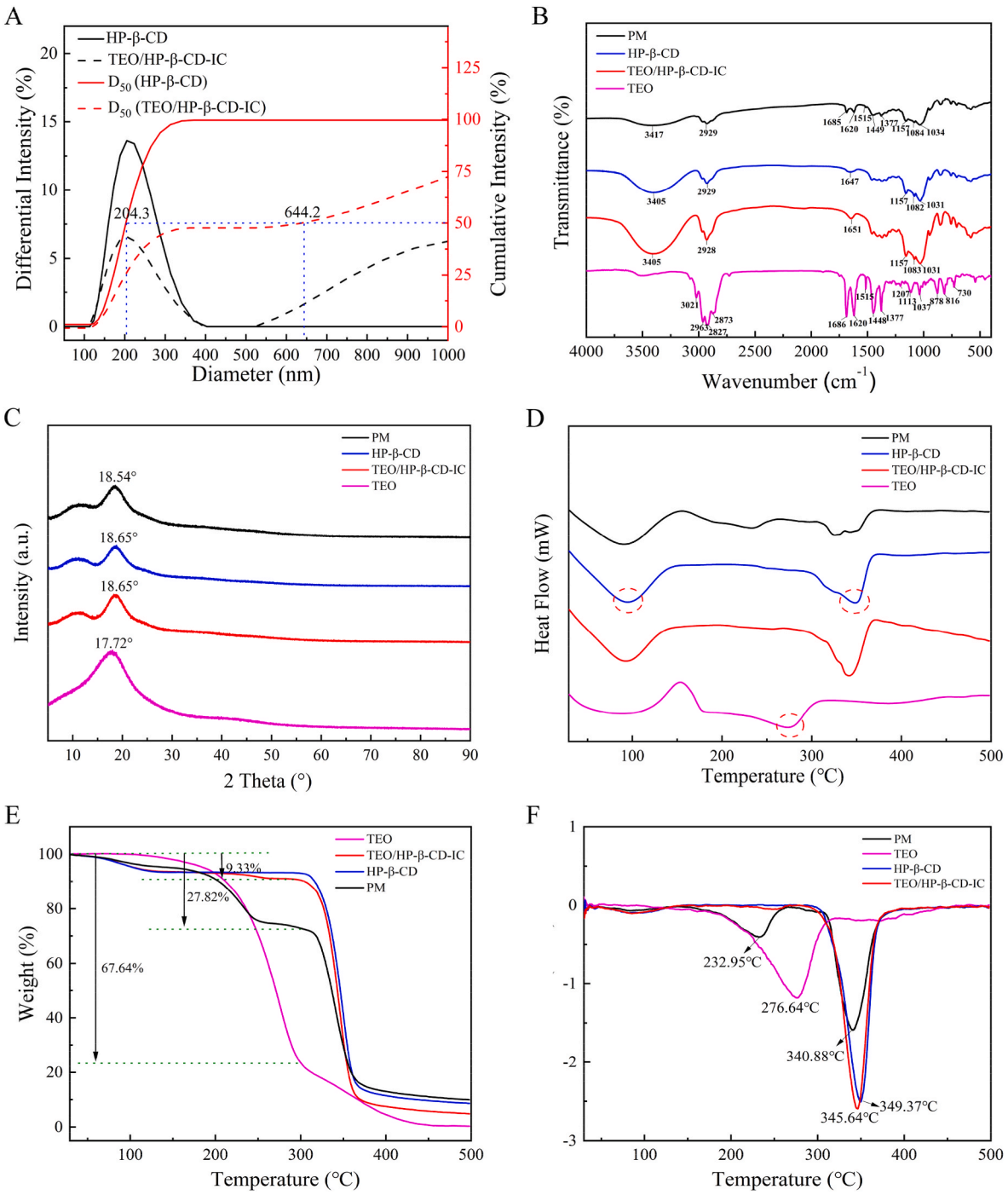

Fig. 2. (A) Particle sizes distribution of HP-β-CD and TEO/HP-β-CD-IC. (B) FT-IR spectra, (C) X-ray diffractograms, (D) DSC curves, (E) TG, and (F) DTG curves of TEO, HP-β-CD, PM, and TEO/HP-β-CD-IC.

TEO, suggesting that TEO was completely embedded in HP-β-CD.

3.2.6. DSC analysis

Whether TEO is embedded in TEO/HP-β-CD-IC was further investigated by DSC to compare HP-β-CD-IC and TEO/HP-β-CD-IC (Hadidi et al., 2020). The DSC curves of TEO, HP-β-CD, PM, and TEO/HP-β-CD-IC are shown in Fig. 2D. The DSC curve of HP-β-CD showed two characteristic peaks, corresponding to HP-β-CD dehydration at about 95 °C and decomposition at 349 °C. Meanwhile, the exothermic peak of TEO near 153 °C was caused by the loss of EO quality. TEO exhibited a endothermic peak at 275 °C, attributable to its decomposition. The DSC thermogram of the PM showed the characteristic peaks of HP-β-CD and TEO. In contrast, the DSC thermogram of TEO/HP-β-CD-IC exhibited an endothermic peak related to HP-β-CD, while no characteristic peaks related to TEO, further confirming the successful encapsulation of TEO.

If the encapsulated bioactive material is not fully incorporated into the encapsulated polymer, its DSC thermogram shows a single peak for each compound (bioactive substance and polymer). If there is no EO–NP interaction, the peak characteristics of the package cannot be observed (Hadidi et al., 2020).

3.2.7. TG analysis

TG analysis is a thermal analysis method in which changes in the

physicochemical properties of materials are measured on the basis of the increase in temperature or changes over time (Zhu et al., 2014). The thermal stability of TEO, HP-β-CD, PM, and TEO/HP-β-CD-IC were investigated by TG. In the TGA curves (Fig. 2E), the pure HP-β-CD exhibited a two-stage weight loss: water loss at <135 °C and main HP-β-CD molecule degradation at >296 °C. Due to volatility, the free TEO showed a 67.64% weight loss at 30−300 °C, indicating its thermal sensibility. Meanwhile, TEO/HP-β-CD-IC also showed water loss between 30 and 300 °C, with a mass loss equivalent to 9.33% of the total sample, implying that encapsulation might have protected TEO from thermal degradation. Moreover, the TG curve of TEO/HP-β-CD-IC showed thermal properties similar to those of HP-β-CD, in contrast to obvious difference between PM and TEO/HP-β-CD-IC in TG curves. In DTG curves (Fig. 2F), thermal decomposition occurred at both 30−257 °C and 315−365 °C for PM, 349.37 °C and 345.64 °C for HP-β-CD and TEO/HP-β-CD-IC, respectively, and 276.64 °C for TEO. These observations showed the enhanced thermal stability of TEO present in the HP-β-CD cavity, indicating that IC can effectively and stably encapsulate foreign molecules even at high temperatures, thereby improving their thermal stability and protecting EOs from evaporation (Cao et al., 2021; Guimaraes et al., 2015).

3.3. Release kinetics of TEO from TEO/HP-β-CD-IC

The IC release behavior is related to temperature and RH. Fig. 3 shows the time course of TEO release from TEO/HP-β-CD-IC under different temperature and RH conditions. At different time intervals, the relative amount of TEO/HP-β-CD-IC released is expressed as the percentage of TEO released. Initially, a certain release amount was noted, which might be related to the adhesion of a small part of TEO on the surface of HP-β-CD. In a previous study (Shi et al., 2019), the initial release was attributed to the amorphous region of the microcapsule. Compared with the crystalline region, the amorphous region had a loose structure and could be easily affected by water vapor, so both temperature and RH had significant effects on TEO release.

In Fig. 3, the release of TEO from TEO/HP-β-CD-IC was seen to increase with the increase of RH and temperature. When exposed to 4 °C temperature and 0% RH, TEO/HP-β-CD-IC showed the lowest TEO release amount (Fig. 3A).

At the same temperature, the TEO release rate from TEO/HP-β-CD-IC was significantly higher at 75% RH than at 0% RH. Specifically, the TEO release rate reached 23.8% within 9 days at 40 °C and 0% RH, but within 1 day as RH increased to 75%, much faster than the release at 0% RH. Seo et al. (2010) attributed this to that high RH may cause the partial dissolution of CD and change its molecular structure, inferring that the TEO release rate is related to the RH around TEO/HP-β-CD-IC (i.e., the percentage of TEO release increases with the increase of RH). Under the same RH, a high-temperature environment accelerated TEO release, and the percentage of TEO released at equilibrium was also higher than that at low RH. For example, at 45% RH, the TEO release percentage reached 28.9% at 40 °C, but could only reach 19.6% at 4 °C. Loganathan et al. (2014) reported that a higher temperature promoted the release rate, presumably because heat accelerated molecular velocity. In the present study, the TEO release percentage reached equilibrium in ~21 and 9 days at 4 and 27 °C, respectively, but in 5 days at 40 °C and 0% RH.

Niu et al. (2020) and Yin et al. (2021) used Avrami's model to fit the releasing process of the flavoring substance in IC:

$$R = exp\,[-(kt)^n] \quad (5)$$

where R is the release rate of TEO at time t; *t*, storage time; k, release rate constant; *n*, release mechanism parameter. Theoretically, $n < 0.54$ indicates a kinetic reaction where diffusion is hindered (i.e., release *via* limited diffusion), and $n = 0.54$–1 indicates the release *via* the combination of limited diffusion and first-order reaction.

However, many controllable release systems do not follow a pure diffusion process, so several other methods have been developed to consider other possible underlying mechanisms. The Power Law model is usually used to describe the Fickian and non-Fickian release behavior, with a focus on the first part of the release curve ($M_t/M_\infty < 60\%$) (Estevez-Areco et al., 2018):

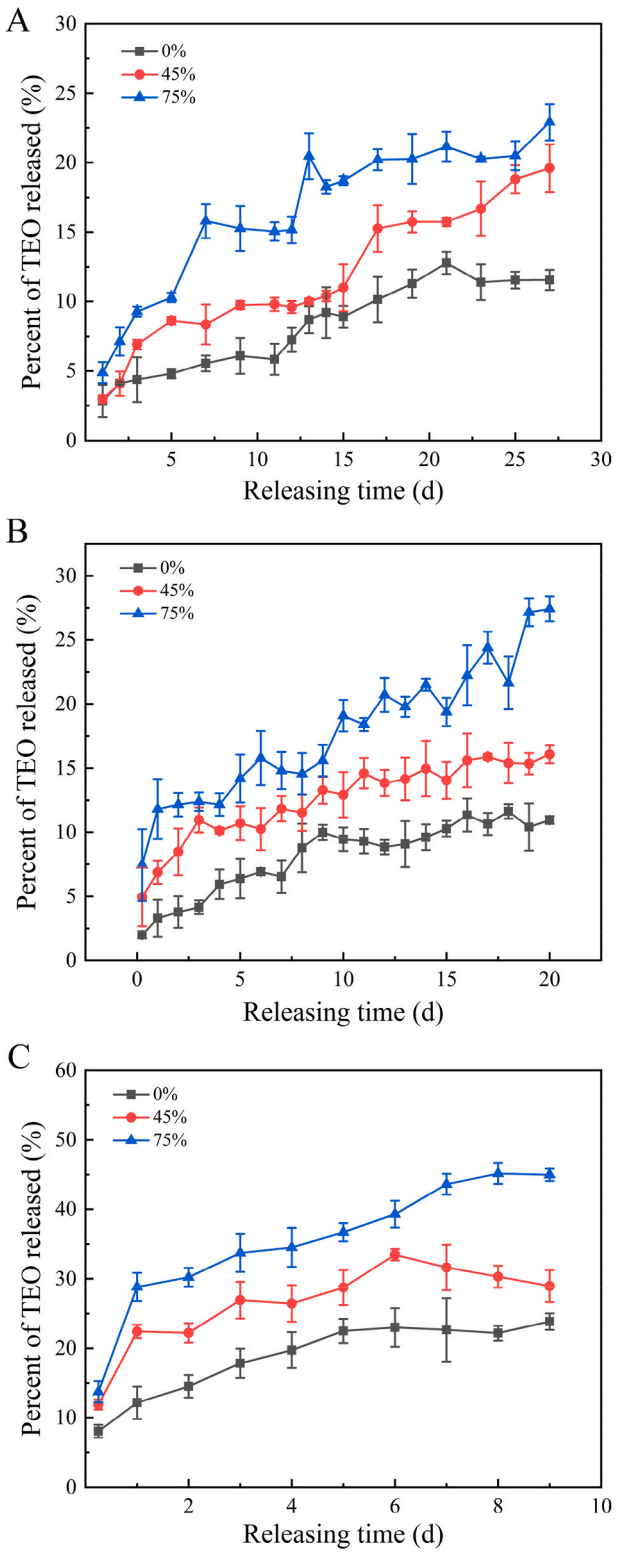

Fig. 3. Effects of RH (0%, 45%, and 75%) and temperature (4, 27, and 40 °C) on the controlled TEO release from TEO/HP-β-CD-IC. (A) 4, (B) 27, and (C) 40 °C.

$$\frac{M_t}{M_\infty} = \mathrm{k}t^n \quad (6)$$

where $\frac{M_t}{M_\infty}$ is the amount of TEO released at time t divided by the amount at equilibrium; k, the kinetic constant; n, release mechanism parameter. Theoretically, $n = \sim 0.45$ indicates release *via* Fick's diffusion, $n = \sim 0.89$ exhibits release *via* the disintegration of CD particles, and $n =$ 0.45–0.89 represents abnormal release.

Another alternative method for describing release behavior is the empirical Weibull function (Estevez-Areco et al., 2018):

$$\frac{M_t}{M_\infty} = 1\text{-}exp\left(a.t^b\right) \quad (7)$$

where $\frac{M_t}{M_\infty}$ is the amount of TEO released at time t divided by the amount at equilibrium; a and b, constants; b, also release mechanism parameter. Theoretically, $b < 0.75$ means the release *via* Fick's diffusion; $b = 0.75$–1 indicates release *via* CD particle disintegration; $b > 1$ shows the release mechanism is complicated.

Fig. 3 presents the TEO release curves fitted to the aforementioned three models, and the related parameters are shown in Table 3. Here, the release rates (n, a, b, and k) of each model were calculated by linear regression analysis, and the correlation coefficient (R^2) was used to evaluate the fitting accuracy. Under different temperature and RH conditions, TEO release could be fitted by these models. The release rate constant k was an important index to characterize the TEO release rate from TEO/HP-β-CD-IC. Under 40 °C, 0% RH, and 45% RH, the TEO release exceeded 60% in a short period.

The Avrami's model could well fit the TEO release kinetics ($R^2 >$ 0.9). In the Avrami's model, except for the conditions of 4 °C and 45% RH, the other n values were all <0.54, indicating that TEO/HP-β-CD-IC followed the release of limited diffusion under these conditions. The TEO release rate was mainly related to the diffusion behavior of TEO molecules from the inside of the microcapsule aggregates. Under the conditions of 40 °C and 45% RH, the n value was between 0.54 and 1, indicating release *via* a combination of limited diffusion and first-order reaction.

These results indicated that TEO release mainly depended on the concentration difference between microcapsules and air. When RH and storage temperature increased, the k value increased. Likewise, the TEO release rate increased with the increase of RH and storage temperature, allowing the rapid release of TEO from TEO/HP-β-CD-IC. In contrast, a low k value indicated that TEO was slowly released from TEO/HP-β-CD-IC. Under high RH, HP-β-CD could be dissolved by absorbing water, resulting in the decomposition of TEO/HP-β-CD-IC during storage. When water begins penetrating particle surfaces, cracks will appear near these surfaces, leading to TEO release (Seo et al., 2010). Overall, the k value was seen to increase with the increase of RH and storage temperature, consistent with the conclusion drawn in Fig. 3.

The Weibull model fitting results were similar to those of the Avrami's model. Under the conditions of 4 °C, 0% and 45% RH, the b values were 0.776 and 0.797, respectively, indicating TEO release *via* the disintegration of CD aggregate particles. Under other conditions, the b value was <0.75, indicating TEO release *via* Fick's diffusion. Comparison of k values under different temperature conditions revealed the increase of k in a temperature-dependent manner. In the Power Law model, only in the case of TEO release at 4 °C, the n values were in the range of 0.45–0.89, indicating abnormal release, and in the remaining six conditions, the n values were all <0.45, indicating TEO release *via* Fick's diffusion.

Therefore, TEO/HP-β-CD-IC showed the lowest TEO release rate under low temperature (4 °C) and low RH (0%) conditions, while the largest TEO release rate at 40 °C with 75% RH, indicating that TEO release could be controlled by changing RH and temperature, because β-CD steric hindrance may protect the volatilization of volatile compounds and adjust their release according to environmental conditions (Da Rocha Neto et al., 2018).

4. Conclusion

In this study, the optimal process conditions for embedding TEO in HP-β-CD were obtained using an orthogonal experiment design. The prepared TEO/HP-β-CD-IC appeared as irregular block structure, with D_{50} particle size of 644.2 nm and a positively charged surface. The ^{1}H NMR, FT-IR, XRD, and DSC results showed that TEO/HP-β-CD-IC was successfully prepared, and the TGA results indicated that microencapsulation could improve TEO thermal stability. Moreover, the models of Avrami, Weibull, and Power Law were used to analyze the TEO release kinetics from TEO/HP-β-CD-IC under different RH and temperature conditions. TEO showed the release *via* limited diffusion in the Avrami model and the release *via* Fick's diffusion law in the Weibull and Power Law models. Overall, the higher the ambient temperature and RH, the higher the TEO release rate from the microcapsules, indicating timely TEO release from microcapsules can be achieved by regulating temperature, RH, and time. There is great potential to apply TEO/HP-β-CD-IC in the active food packaging. Therefore, the antibacterial characteristics of the IC and their impact on food preservation will be investigated further.

CRediT authorship contribution statement

Yueyue Qiang: Conceptualization, Methodology, Investigation, Data curation, Writing – original draft, preparation. **Hang Wei:** Investigation, Formal analysis. **Biao Huang:** Investigation, Resources. **Hongfei Chi:** Investigation, Resources. **Jianwei Fu:** Conceptualization, Supervision, Project administration, Funding acquisition, Shaoxiao Zeng, Investigation, Formal analysis, Visualization.

Declaration of competing interest

The authors declare that they have no known competing financial interests or personal relationships that could have appeared to influence

Table 3
Parameters for TEO release fitted with Avrami, Weibull, and Power Law models.

Temperature (°C)	RH (%)<	Avrami			Weibull			Power Law		
		k	n	R^2	a	b	R^2	k	n	R^2
4	0	4.570×10^{-4}	0.471	0.921	8.746×10^{-2}	0.776	0.932	0.2006	0.455	0.924
	45	1.791×10^{-3}	0.552	0.933	6.692×10^{-2}	0.797	0.925	0.1539	0.526	0.936
	75	2.472×10^{-3}	0.486	0.959	0.1051	0.699	0.952	0.2136	0.454	0.958
27	0	3.890×10^{-4}	0.436	0.959	0.1649	0.670	0.901	0.2700	0.423	0.960
	45	1.006×10^{-4}	0.285	0.969	0.2604	0.490	0.914	6.952×10^{-2}	0.270	0.970
	75	9.700×10^{-4}	0.342	0.919	0.1142	0.496	0.917	5.319×10^{-2}	0.318	0.929
40	0	2.566×10^{-3}	0.343	0.979	0.0859	0.392	0.940	–	–	–
	45	4.412×10^{-3}	0.284	0.902	0.8666	0.474	0.913	0.554	0.272	0.946
	75	2.855×10^{-2}	0.361	0.952	0.6368	0.503	0.957	0.526	0.305	0.944

the work reported in this paper.

Data availability

Data will be made available on request.

Acknowledgements

This work was supported by the Spark Technology Project of Fujian Province (Grant No. 2023S0057), China; Public Welfare Project Program of Fujian Province (Grant No. 2019R1002-5 and 2021R102205), China; the Science and Technology Innovation Team Construction Project of FAAS (Grant No. CXTD2021011-1); the Team Project of Quanzhou City for High-level Talents (Grant No. 2019CT008), Fujian Province, China; the "5511" Collaborative innovation Project (Grant No. XTCXGC2021020), China.

Appendix A. Supplementary data

Supplementary data to this article can be found online at https://doi.org/10.1016/j.crfs.2023.100668.

References

Acevedo-Fani, A., Salvia-Trujillo, L., Rojas-Graü, M.A., Martín-Belloso, O., 2015. Edible films from essential-oil-loaded nanoemulsions: physicochemical characterization and antimicrobial properties. Food Hydrocolloids 47, 168–177. https://doi.org/10.1016/j.foodhyd.2015.01.032.

Adhikari, S., Daftardar, S., Fratev, F., Rivera, M., Sirimulla, S., Alexander, K., Boddu, S.H. S., 2018. Elucidation of the orientation of selected drugs with 2-hydroxylpropyl-beta-cyclodextrin using 2D-NMR spectroscopy and molecular modeling. Int. J. Pharm. 545 (1–2), 357–365. https://doi.org/10.1016/j.ijpharm.2018.05.016.

Ban, Z., Zhang, J., Li, L., Luo, Z., Wang, Y., Yuan, Q., Zhou, B., Liu, H., 2020. Ginger essential oil-based microencapsulation as an efficient delivery system for the improvement of Jujube (*Ziziphus jujuba* Mill.) fruit quality. Food Chem. 306, 125628 https://doi.org/10.1016/j.foodchem.2019.125628.

Cao, C., Wei, D., Xu, L., Hu, J., Qi, J., Zhou, Y., 2021. Characterization of tea tree essential oil and large-ring cyclodextrins (CD_9 -CD_{22}) inclusion complex and evaluation of its thermal stability and volatility. J. Sci. Food Agric. 101 (7), 2877–2883. https://doi.org/10.1002/jsfa.10919.

Chumroenphat, T., Somboonwatthanakul, I., Saensouk, S., Siriamornpun, S., 2021. Changes in curcuminoids and chemical components of turmeric (*Curcuma longa* L.) under freeze-drying and low-temperature drying methods. Food Chem. 339, 128121 https://doi.org/10.1016/j.foodchem.2020.128121.

Commission, N.P., 2015. Chinese Pharmacopoeia. China Medical Science and Technology Press, Beijing, pp. 2300–2301.

Da Rocha Neto, A.C., de Oliveira da Rocha, A.B., Maraschin, M., Di Piero, R.M., Almenar, E., 2018. Factors affecting the entrapment efficiency of β-cyclodextrins and their effects on the formation of inclusion complexes containing essential oils. Food Hydrocolloids 77, 509–523. https://doi.org/10.1016/j.foodhyd.2017.10.029.

De Santana, N.A., da Silva, R.C.S., Fourmentin, S., dos Anjos, K.F.L., Ootan, M.A., da Silva, A.G., Pereira Araújo, B.G., dos Santos Correia, M.T., da Silva, M.V., Machado, G., 2020. Synthesis, characterization and cytotoxicity of the Eugenia brejoensis essential oil inclusion complex with β-cyclodextrin. J. Drug Deliv. Sci. Technol. 60, 101876 https://doi.org/10.1016/j.jddst.2020.101876.

Estevez-Areco, S., Guz, L., Candal, R., Goyanes, S., 2018. Release kinetics of rosemary (*Rosmarinus officinalis*) polyphenols from polyvinyl alcohol (PVA) electrospun nanofibers in several food simulants. Food Packag. Shelf Life 18, 42–50. https://doi.org/10.1016/j.fpsl.2018.08.006.

Ferreira, F.D., Kemmelmeier, C., Arroteia, C.C., da Costa, C.L., Mallmann, C.A., Janeiro, V., Ferreira, F.M., Mossini, S.A., Silva, E.L., Machinski Jr., M., 2013. Inhibitory effect of the essential oil of *Curcuma longa* L. and curcumin on aflatoxin production by *Aspergillus flavus* Link. Food Chem. 136 (2), 789–793. https://doi.org/10.1016/j.foodchem.2012.08.003.

Gould, S., Scott, R.C., 2005. 2-Hydroxypropyl-beta-cyclodextrin (HP-beta-CD): a toxicology review. Food Chem. Toxicol. 43 (10), 1451–1459. https://doi.org/10.1016/j.fct.2005.03.007.

Guimaraes, A.G., Oliveira, M.A., Alves Rdos, S., Menezes Pdos, P., Serafini, M.R., Araujo, A.A., Bezerra, D.P., Quintans Junior, L.J., 2015. Encapsulation of carvacrol, a monoterpene present in the essential oil of oregano, with beta-cyclodextrin, improves the pharmacological response on cancer pain experimental protocols. Chem. Biol. Interact. 227, 69–76. https://doi.org/10.1016/j.cbi.2014.12.020.

Hadidi, M., Pouramin, S., Adinepour, F., Haghani, S., Jafari, S.M., 2020. Chitosan nanoparticles loaded with clove essential oil: characterization, antioxidant and antibacterial activities. Carbohydr. Polym. 236, 116075 https://doi.org/10.1016/j.carbpol.2020.116075.

Lertsutthiwong, P., Noomun, K., Jongaroonngamsang, N., Rojsitthisak, P., Nimmannit, U., 2008. Preparation of alginate nanocapsules containing turmeric oil. Carbohydr. Polym. 74 (2), 209–214. https://doi.org/10.1016/j.carbpol.2008.02.009.

Lertsutthiwong, P., Rojsitthisak, P., Nimmannit, U., 2009. Preparation of turmeric oil-loaded chitosan-alginate biopolymeric nanocapsules. Mater. Sci. Eng. C. 29 (3), 856–860. https://doi.org/10.1016/j.msec.2008.08.004.

Li, L., Song, W., Shen, C., Dong, Q., Wang, Y., Zuo, S., 2020. Active packaging film containing oregano essential oil microcapsules and their application for strawberry preservation. J. Food Process. Preserv. 44 (10) https://doi.org/10.1111/jfpp.14799.

Li, Z., Lin, S., An, S., Liu, L., Hu, Y., Wan, L., 2019. Preparation, characterization and anti-aflatoxigenic activity of chitosan packaging films incorporated with turmeric essential oil. Int. J. Biol. Macromol. 131, 420–434. https://doi.org/10.1016/j.ijbiomac.2019.02.169.

Lima, B.D.S., Campos, C.A., da Silva Santos, A.C.R., Santos, V.C.N., Trindade, G., Shanmugam, S., Pereira, E.W.M., Marreto, R.N., Duarte, M.C., Almeida, J., Quintans, J.S.S., Quintans Jr., L.J., Araujo, A.A.S., 2019. Development of morin/hydroxypropyl-beta-cyclodextrin inclusion complex: enhancement of bioavailability, antihyperalgesic and anti-inflammatory effects. Food Chem. Toxicol. 126, 15–24. https://doi.org/10.1016/j.fct.2019.01.038.

Liu, Y., Zhang, G., Zhu, G., Aikemu, A., Ai, J., Li, D., 2018. Using the box-behnken response surface method to optimize the preparation and characterization of lavender and fennel volatile oil β-cyclodextrin form inclusion complex, 0.0. 4(02), 54-61. https://doi.org/10.4103/wjtcm.wjtcm_9_18.

Loganathan, S., Tikmani, M., Edubilli, S., Mishra, A., Ghoshal, A.K., 2014. CO_2 adsorption kinetics on mesoporous silica under wide range of pressure and temperature. Chem. Eng. J. 256, 1–8. https://doi.org/10.1016/j.cej.2014.06.091.

Matshetshe, K.I., Parani, S., Manki, S.M., Oluwafemi, O.S., 2018. Preparation, characterization and *in vitro* release study of beta-cyclodextrin/chitosan nanoparticles loaded *Cinnamomum zeylanicum* essential oil. Int. J. Biol. Macromol. 118 (Pt A), 676–682. https://doi.org/10.1016/j.ijbiomac.2018.06.125.

Mehran, M., Masoum, S., Memarzadeh, M., 2020. Microencapsulation of *Mentha spicata* essential oil by spray drying: optimization, characterization, release kinetics of essential oil from microcapsules in food models. Ind. Crops Prod. 154, 112694 https://doi.org/10.1016/j.indcrop.2020.112694.

Mustapha, F.A., Jai, J., Nik Raikhan, N.H., Sharif, Z.I.M., Yusof, N.M., 2019. Response surface methodology analysis towards biodegradability and antimicrobial activity of biopolymer film containing turmeric oil against *Aspergillus niger*. Food Control 99, 106–113. https://doi.org/10.1016/j.foodcont.2018.12.042.

Niu, Y., Deng, J., Xiao, Z., Kou, X., Zhu, G., Liu, M., Liu, S., 2020. Preparation and slow release kinetics of apple fragrance/β-cyclodextrin inclusion complex. J. Therm. Anal. Calorim. 143 (5), 3775–3781. https://doi.org/10.1007/s10973-020-09292-9.

Noghabi, M.S., Molaveisi, M., 2020. Microencapsulation of Persian gum as a novel wall material for the fast-release of cinnamon essential oil in the simulated saliva medium: characterization of microcapsules and modeling the kinetics of release. Bioact. Carbohydr. Diet. Fibre., 100250 https://doi.org/10.1016/j.bcdf.2020.100250.

Qiu, N., Cheng, X., Wang, G., Wang, W., Wen, J., Zhang, Y., Song, H., Ma, L., Wei, Y., Peng, A., Chen, L., 2014. Inclusion complex of barbigerone with hydroxypropyl-beta-cyclodextrin: preparation and *in vitro* evaluation. Carbohydr. Polym. 101, 623–630. https://doi.org/10.1016/j.carbpol.2013.09.035.

Rakmai, J., Cheirsilp, B., Mejuto, J.C., Torrado-Agrasar, A., Simal-Gándara, J., 2017. Physico-chemical characterization and evaluation of bio-efficacies of black pepper essential oil encapsulated in hydroxypropyl-beta-cyclodextrin. Food Hydrocolloids 65, 157–164. https://doi.org/10.1016/j.foodhyd.2016.11.014.

Seo, E.J., Min, S.G., Choi, M.J., 2010. Release characteristics of freeze-dried eugenol encapsulated with beta-cyclodextrin by molecular inclusion method. J. Microencapsul. 27 (6), 496–505. https://doi.org/10.3109/02652041003681398.

Shetta, A., Kegere, J., Mamdouh, W., 2019. Comparative study of encapsulated peppermint and green tea essential oils in chitosan nanoparticles: encapsulation, thermal stability, *in-vitro* release, antioxidant and antibacterial activities. Int. J. Biol. Macromol. 126, 731–742. https://doi.org/10.1016/j.ijbiomac.2018.12.161.

Shi, L., Hopfer, H., Ziegler, G.R., Kong, L., 2019. Starch-menthol inclusion complex: structure and release kinetics. Food Hydrocolloids 97. https://doi.org/10.1016/j.foodhyd.2019.105183.

Wang, X., Wang, K., Lu, Z., Wang, T., 2015. Preparation, stability and antifungal activity of *Curcuma longa* volatile oil/hydroxypropyl-β-cyclodextrin inclusion compound. Chin. J. New Drugs Clin. Remedies 38 (7), 433–439. https://doi.org/10.14109/j.cnki.xyylc.2019.07.011.

Wei, Y., Zhang, J., Zhou, Y., Bei, W., Li, Y., Yuan, Q., Liang, H., 2017. Characterization of glabridin/hydroxypropyl-beta-cyclodextrin inclusion complex with robust solubility and enhanced bioactivity. Carbohydr. Polym. 159, 152–160. https://doi.org/10.1016/j.carbpol.2016.11.093.

Wissing, S.A., Kayser, O., Muller, R.H., 2004. Solid lipid nanoparticles for parenteral drug delivery. Adv. Drug Deliv. Rev. 56 (9), 1257–1272. https://doi.org/10.1016/j.addr.2003.12.002.

Yang, X., Gao, N., Hu, L., Li, J., Sun, Y., 201. Development and evaluation of novel microcapsules containing poppy-seed oil using complex coacervation. J. Food Eng.. 161, 87-93. https://doi.org/10.1016/j.jfoodeng.2015.03.027. .

Yao, Y., Xie, Y., Hong, C., Li, G., Shen, H., Ji, G., 2014. Development of a myricetin/hydroxypropyl-beta-cyclodextrin inclusion complex: preparation, characterization, and evaluation. Carbohydr. Polym. 110, 329–337. https://doi.org/10.1016/j.carbpol.2014.04.006.

Yin, H., Wang, C., Yue, J., Deng, Y., Jiao, S., Zhao, Y., Zhou, J., Cao, T., 2021. Optimization and characterization of 1,8-cineole/hydroxypropyl-β-cyclodextrin

inclusion complex and study of its release kinetics. Food Hydrocolloids 110, 106159. https://doi.org/10.1016/j.foodhyd.2020.106159.
Zhou, W., He, Y., Liu, F., Liao, L., Huang, X., Li, R., Zou, Y., Zhou, L., Zou, L., Liu, Y., Ruan, R., Li, J., 2021. Carboxymethyl chitosan-pullulan edible films enriched with galangal essential oil: characterization and application in mango preservation. Carbohydr. Polym. 256, 117579 https://doi.org/10.1016/j.carbpol.2020.117579.
Zhu, G., Xiao, Z., Zhou, R., Zhu, Y., 2014. Study of production and pyrolysis characteristics of sweet orange flavor-beta-cyclodextrin inclusion complex. Carbohydr. Polym. 105, 75–80. https://doi.org/10.1016/j.carbpol.2014.01.060.